PNAS RESEARCH ARTICLE | MEDICAL SCIENCES

# Endothelial VWF is critical for the pathogenesis of vaso-occlusive episode in a mouse model of sickle cell disease

Huiping Shi[a,b], Bojing Shao[a], Liang Gao[a], Thamizhiniyan Venkatesan[a], John Michael McDaniel[a], Meixiang Zhou[a], Samuel McGee[a], Pengchun Yu[a], Jasimuddin Ahamed[a], Janna Journeycake[c], James N. George[d], and Lijun Xia[a,b,1]

Edited by Barry Coller, The Rockefeller University, New York, NY; received May 4, 2022; accepted July 18, 2022

**Vaso-occlusive episode (VOE) is a common and critical complication of sickle cell disease (SCD). Its pathogenesis is incompletely understood. von Willebrand factor (VWF), a multimeric plasma hemostatic protein synthesized and secreted by endothelial cells and platelets, is increased during a VOE. However, whether and how VWF contributes to the pathogenesis of VOE is not fully understood. In this study, we found increased VWF levels during tumor necrosis factor (TNF)–induced VOE in a humanized mouse model of SCD. Deletion of endothelial VWF decreased hemolysis, vascular occlusion, and organ damage caused by TNF-induced VOE in SCD mice. Moreover, administering ADAMTS13, the VWF-cleaving plasma protease, reduced plasma VWF levels, decreased inflammation and vaso-occlusion, and alleviated organ damage during VOE. These data suggest that promoting VWF cleavage via ADAMTS13 may be an effective treatment for reducing hemolysis, inflammation, and vaso-occlusion during VOE.**

sickle cell disease | vaso-occlusive episode | von Willebrand factor

## Significance

Current main treatments for sickle cell disease (SCD), such as hydroxyurea, L-glutamine, and crizanlizumab, reduce the frequency of vaso-occlusive episode (VOE). However, a considerable number of individuals with SCD still develop VOE. For example, although the rate was significantly reduced, VOE still occurred in 64% of individuals with SCD treated with prophylactic use of high-dose crizanlizumab, a P-selectin targeting antibody therapy newly approved by the Food and Drug Administration. Once VOE occurs, treatments are limited to supportive therapies. Thus, a better understanding of mechanisms underlying VOE pathogenesis and development of new therapies are needed to effectively manage VOE. Our study indicates that promoting von Willebrand factor cleavage by ADAMTS13 may be an effective treatment for alleviating VOE-associated organ damage.

Sickle cell disease (SCD) is the most common inherited hematologic disorder in the United States (1). It is associated with severe complications and increased mortality (2). Individuals with SCD often suffer from painful and potentially fatal vaso-occlusive episodes (VOEs). A VOE is the result of microvascular occlusion caused by interactions among sickle red blood cells (RBCs), vascular endothelial cells (ECs), platelets, and neutrophils (3–5).

Currently, there are several medications for reducing the frequency of VOE, which include hydroxyurea, L-glutamine, and crizanlizumab (6–8). However, despite these relatively effective therapies, VOE still commonly occurs in individuals with SCD. For example, 64% of individuals with SCD treated with prophylactic crizanlizumab, an antibody therapy newly approved by the Food and Drug Administration (FDA) targeting the adhesion molecule P-selectin, still developed VOE, albeit at a significantly reduced rate (6). In addition, for the pathogenesis of VOE, attention has primarily focused on the sickling-unsickling occurrences that predispose sickle RBCs to fragmentation (9). The molecular pathogenesis of VOE-associated organ injury is incompletely understood. As a result, current available treatments for VOE have been primarily limited to supportive therapies such as analgesia and hydration (10). There are no effective therapies to mitigate organ damage during VOE.

von Willebrand factor (VWF), a multimeric glycoprotein synthesized and secreted by ECs and platelets, is critical for mediating platelet adhesion to the injured vessel wall (11–13). Dysregulation of clot formation has been reported in SCD (14). Previous studies showed VWF-mediated sickle RBC adhesion to human ECs in vitro (15) and increased VWF levels and adhesive activity in individuals with SCD during steady state (16–18). Moreover, the amount of hyper-adhesive high molecular weight portion of VWF and its interactions with the platelet receptor GPIb were increased in individuals with SCD when VOE occurred (19). In a previous study, a sheep anti-rat VWF antibody was used to reduce heme-induced vessel stasis in a dorsal skinfold chamber model in SCD mice (20). However, the antibody was not validated for its efficacy to inhibit mouse VWF-mediated thrombosis. Blood stasis in organs other than skin was not analyzed in this study. VWF function is primarily regulated by ADAMTS13, a plasma enzyme that cleaves multimeric VWF at its A2 domain (21, 22). ADAMTS13 deficiency causes increased accumulation of high molecular weight VWF multimers in plasma, which is the etiology of thrombotic thrombocytopenic purpura (TTP) (23). While the causative role of VWF in TTP is well established, the role of VWF in the pathogenesis of VOE remains to be studied.

In this study, we documented that deletion of VWF synthesis in ECs reduced hemolysis, vascular occlusion, and organ damage caused by tumor necrosis factor (TNF)–induced

Author contributions: H.S. and L.X. designed research; H.S., B.S., L.G., T.V., J.M.M., M.Z., S.M., and J.A. performed research; P.Y. contributed new reagents/analytic tools; H.S., L.G., J.A., J.J., and L.X. analyzed data; and H.S., J.N.G., and L.X. wrote the paper.

The authors declare no competing interest.

This article is a PNAS Direct Submission.



See online for related content such as Commentaries.

[1]To whom correspondence may be addressed. Email: lijun-xia@omrf.org.

This article contains supporting information online at http://www.pnas.org/lookup/suppl/doi:10.1073/pnas.2207592119/-/DCSupplemental.

Published August 15, 2022.

VOE in a mouse model of SCD. We also documented that ADAMTS13 treatment effectively reduced plasma VWF, decreased inflammation and vaso-occlusion, and alleviated organ damage during VOE in SCD mice. These data document a critical contributing role of VWF in the pathogenesis of VOE and suggest that VWF cleavage by ADAMTS13 may be an effective therapeutic option for reducing VOE-associated pathological changes.

## Results

**VWF Is Increased during VOE in SCD Mice.** Humanized SCD mice (Townes mice) homozygous for human sickle cell hemoglobin $\beta^S/\beta^S$ (*S/S*, SCD mice) or human wild-type (WT) hemoglobin $\beta^A/\beta^A$ (*A/A*, WT control) were used for this study (24). *S/S* mice exhibit human SCD-like phenotypes, including the presence of sickle RBCs, anemia, and multiorgan damage (*SI Appendix*, Fig. S1). To study the role of VWF in VOE, VOE was induced in *S/S* mice by intraperitoneal injection of 500 ng TNF (25). *S/S* mice with TNF-induced VOE exhibited decreased levels of hemoglobin and platelet counts relative to *A/A* mice (Fig. 1*A*). Plasma VWF levels were significantly increased in *S/S* mice after TNF-induced VOE (Fig. 1*B*) but were unchanged in *A/A* mice treated with 500 ng TNF. After TNF challenge, ischemic and necrotic changes accompanied by inflammatory infiltrates were obvious in the liver of *S/S* mice compared to that of *A/A* mice (*SI Appendix*, Fig. S2). Pathological changes consistent with vaso-occlusions in glomeruli and acute tubular injury, such as glomerulus congestion, tubular luminal dilation, and loss of epithelial cell nucleus, were observed in the kidney of *S/S* mice challenged with TNF relative to controls (*SI Appendix*, Fig. S2). Additionally, increased vaso-occlusions were found in the lung (*SI Appendix*, Fig. S2), heart, and brain (*SI Appendix*, Fig. S3) of *S/S* but not *A/A* mice.

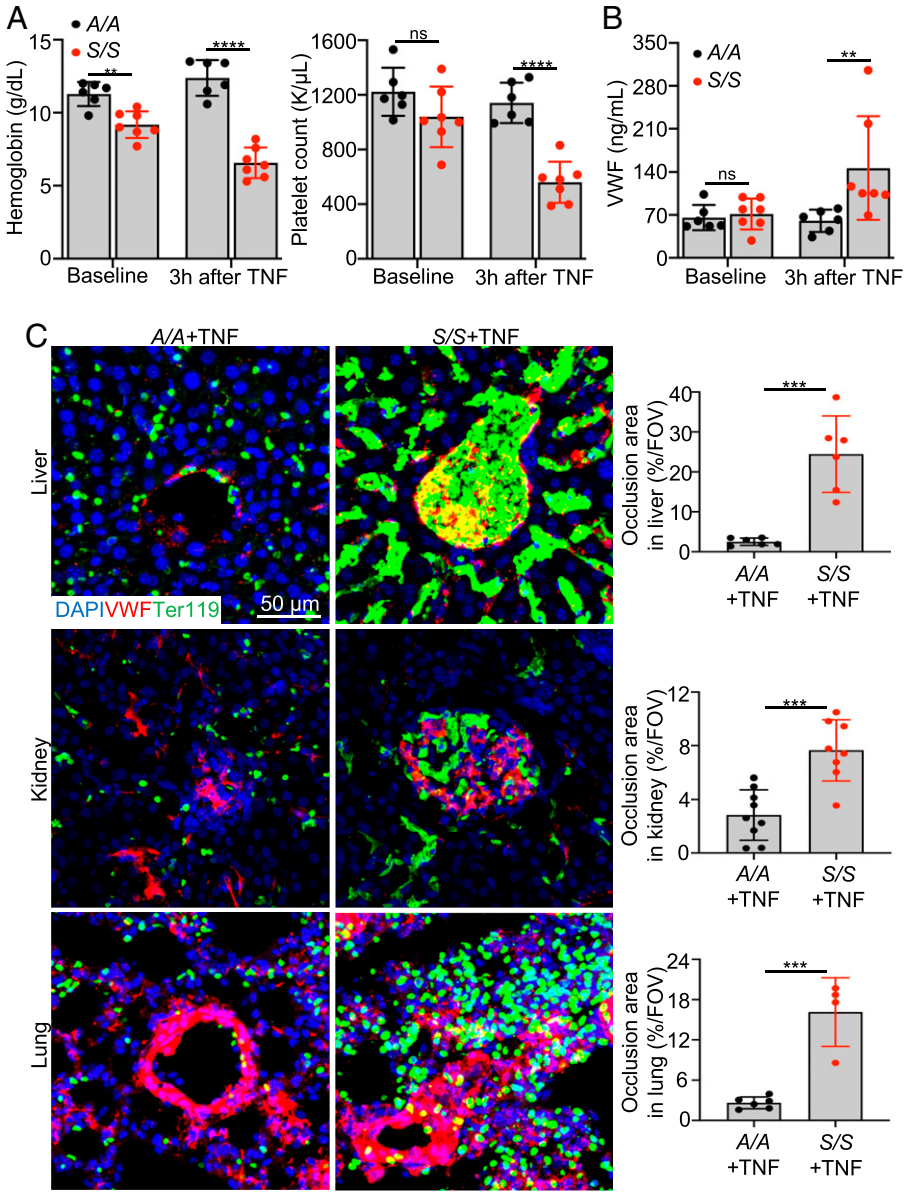


**Fig. 1.** VWF is increased during VOE in SCD mice. (*A*) Hemoglobin levels and platelet counts of *A/A* and *S/S* mice at baseline and 3 h after TNF challenge are shown. Each dot represents one mouse. Data represent mean ± SD. ****$P < 0.0001$; ns, nonsignificant, repeated measures 2-way ANOVA. (*B*) Plasma VWF levels in *A/A* and *S/S* mice at baseline and 3 h after TNF challenge are shown. Each dot represents one mouse. Data represent mean ± SD. **$P < 0.01$; ns, nonsignificant, repeated measures 2-way ANOVA. (*C*) Representative immunofluorescence images of cryosections of liver, kidney, and lung collected from *A/A* and *S/S* mice at 3 h after VOE induction. Scale bar, 50 μm. Quantification of the percentage of vaso-occlusion area per field of view (FOV) using ImageJ is shown on the right. $n = 4$ mice per genotype. Data represent mean ± SD. ***$P < 0.001$, two-tailed, unpaired Student's *t* test.

Increased inflammatory infiltrates were observed in *S/S* mice at baseline, and this was further increased at 3 h after VOE induction, while *A/A* mice had no obvious inflammation (*SI Appendix*, Fig. S4 *A* and *B*). Immunofluorescence staining revealed significantly increased VWF staining and vaso-occlusions in liver, kidney, lung (Fig. 1*C*), heart, and brain (*SI Appendix*, Fig. S3) of *S/S* mice, while *A/A* mice showed no vaso-occlusion. To validate these findings, VOE was induced by challenging mice with hypoxia for 10 h (8% $O_2$) followed by reoxygenation for 2 h. Similarly, *S/S* mice exhibited increased VWF staining in major organs compared with control mice (*SI Appendix*, Fig. S5). These results show that VWF is increased during VOE in *S/S* mice, suggesting the potential contribution of VWF to VOE pathogenesis in SCD.

**Endothelial VWF Deletion in Mice Alleviates VOE.** The majority of circulating VWF is derived from vascular ECs (26). We generated $S/S^{EC\ KO}$ mice (*S/S* mice lacking endothelial VWF) by transplanting *S/S* bone marrow into $VWF^{-/-}$ mice to determine the importance of EC-derived VWF in VOE. WT mice were transplanted with *S/S* bone marrow as controls ($S/S^{EC\ VWF}$). At 4 mo after transplantation, blood smear was performed, and sickle RBCs were found in the peripheral blood of both $S/S^{EC\ VWF}$ and $S/S^{EC\ KO}$ mice, indicating the success of transplantation (*SI Appendix*, Fig. S6*A*). Complete engraftment of donor hematopoietic cells was verified by analysis of lysed RBC solution and documentation of hemoglobin S using high-performance liquid chromatography at 4 mo after transplantation (Fig. 2*A*). VWF multimer analysis confirmed that $S/S^{EC\ KO}$ mice expressed platelet-derived VWF but showed minimal plasma VWF (Fig. 2*B*), which is consistent with the literature that very little platelet-synthesized VWF is released into the circulation until platelet activation (26). Compared to $S/S^{EC\ VWF}$ mice, $S/S^{EC\ KO}$ mice showed less severe anemia both at basal level and during TNF-induced VOE (Fig. 2*C*). Importantly, sickle RBC occlusion and inflammation in the liver were alleviated in $S/S^{EC\ KO}$ mice compared to $S/S^{EC\ VWF}$ mice after TNF challenge (Fig. 2 *D* and *E*). Hematoxylin/eosin (H&E) and immunofluorescence staining showed reduced TNF-induced vascular occlusion in the liver, kidney, lung, heart, and brain of $S/S^{EC\ KO}$ mice relative to that of $S/S^{EC\ VWF}$ mice (Fig. 2*E* and *SI Appendix*, Fig. S6 *B* and *C*). Moreover, immuno-staining showed that $S/S^{EC\ KO}$ mice had significantly reduced inflammatory infiltrates at 3 h after VOE induction compared to $S/S^{EC\ VWF}$ mice (*SI Appendix*, Fig. S4*C*). Trichrome staining showed that *S/S* and $S/S^{EC\ VWF}$ mice exhibited extensive collagen deposition in the liver and kidney, while age- and sex-matched $S/S^{EC\ KO}$ mice had little collagen deposition, similar to that of *A/A* controls (*SI Appendix*, Fig. S7). These results demonstrate that endothelial VWF contributes to VOE pathogenesis and that deletion of endothelial VWF could reduce VOE-related phenotypes.

**ADAMTS13 Injection before VOE Improves Histopathologic Phenotypes of VOE in SCD Mice.** ADAMTS13 reduces VWF prothrombotic activity by cleaving VWF A2 domain. Thus, whether cleavage of VWF by ADAMTS13 protects SCD mice from VOE injury was investigated. *S/S* mice were injected with recombinant ADAMTS13 (3 μg/mouse, intravenously) or vehicle control 15 min before TNF-induced VOE induction. ADAMTS13 significantly reduced liver damage in *S/S* mice compared to control *S/S* mice (*SI Appendix*, Fig. S8*A*). ADAMTS13 pretreatment also significantly decreased plasma levels of VWF antigen (*SI Appendix*, Fig. S8*A*). VWF-positive thrombi and RBC occlusion were reduced in liver (*SI Appendix*, Fig. S8 *B* and *C*) and other major organs (*SI Appendix*, Fig. S9) of ADAMTS13-pretreated mice. Moreover, the inflammatory cytokines interleukin (IL) 1β and IL-12 are known to be increased in individuals with SCD (27–29), but they were significantly reduced by ADAMTS13 injection in SCD mice (*SI Appendix*, Fig. S8*D*), suggesting reduced inflammation in *S/S* mice with ADAMTS13 pretreatment. Immuno-staining showed that *S/S* mice pretreated with ADAMTS13 had reduced inflammatory infiltrates in the liver at 3 h after VOE induction compared to those injected with vehicle (*SI Appendix*, Fig. S8*E*). These results indicate that ADAMTS13 pretreatment reduces ischemic organ injury, inhibits inflammation, decreases vaso-occlusion, and alleviates organ damage during VOE.

**ADAMTS13 Injection after VOE Reduces Pathological Changes Associated with TNF-Induced VOE in SCD Mice.** To determine if ADAMTS13 could effectively reduce VOE-associated organ damage, we treated *S/S* mice with recombinant ADAMTS13 (3 μg/mouse, intravenously) 15 min after VOE induction by TNF. Hemoglobin levels and platelet counts were significantly improved in *S/S* mice treated with ADAMTS13 (Fig. 3*A*). Plasma levels of lactate dehydrogenase (LDH), aspartate aminotransferase (AST), and alanine aminotransferase (ALT) in ADAMTS13-treated *S/S* mice were reduced compared to vehicle-treated *S/S* mice (Fig. 3*B*). Compared to *S/S* mice treated with vehicle, the *S/S* mice injected with ADAMTS13 showed reduced ischemic and inflammatory changes in the liver (Fig. 3*C*). Vaso-occlusions in glomeruli and signs of acute tubular injury, such as loss of epithelial cell nucleus and sloughing of tubular epithelial cells, were reduced in *S/S* mice treated with ADAMTS13 (Fig. 3*C* and *SI Appendix*, Fig. S10*A*). Similarly, vaso-occlusions in the lung, heart, and brain were reduced in *S/S* mice treated with ADAMST13 compared to vehicle-treated *S/S* mice (Fig. 3*C* and *SI Appendix*, Fig. S10*A*). Inflammatory infiltrates were significantly reduced by ADAMTS13 treatment as shown by the decreased staining of CD45 in the liver (Fig. 3*D*). Moreover, intravital spinning disk confocal microscopy real-time imaging demonstrated that *S/S* mice with TNF-induced VOE had greater vaso-occlusion and more adherent platelets in liver sinusoids compared with *A/A* mice (Movies S1 and S2). ADAMTS13 treatment reduced vaso-occlusion and platelet adhesion to sinusoidal ECs in the *S/S* liver with TNF-induced VOE compared with mice without the treatment (*SI Appendix*, Fig. S10*B* and Movies S2 and S3). This result indicates that ADAMTS13 treatment reduces vaso-occlusion, possibly by cleaving VWF and reducing platelet adhesion to sinusoidal endothelium in the liver.

**Platelets and Fibrin Are Present in TNF-Induced VOE in SCD Mice.** Our data support that the formation of platelet-VWF clusters entrapping RBCs is critical for the pathogenesis of VOE. When liver tissue sections were stained with antibodies to platelet and fibrin(ogen), platelet- and fibrin-positive thrombi were frequently detected in TNF-induced VOE of *S/S* mice compared with *S/S* mice at baseline (Fig. 4*A*). Most of these thrombi were found within RBC occlusions as indicated by differential interference contrast microscopy imaging (Fig. 4*B*). Moreover, ADAMTS13 treatment significantly reduced the formation of platelet- and fibrin-positive thrombi and RBC entrapping (Fig. 4 *A* and *B*), which is consistent with improvement of platelet count after ADAMTS13 treatment (Fig. 3*A*).

## Discussion

VOE is a multicellular and multistep pathological process. Previous studies show that VWF level and activity are increased in individuals with SCD at steady state (16–18) and are further elevated when VOE occurs (19). However, whether and how

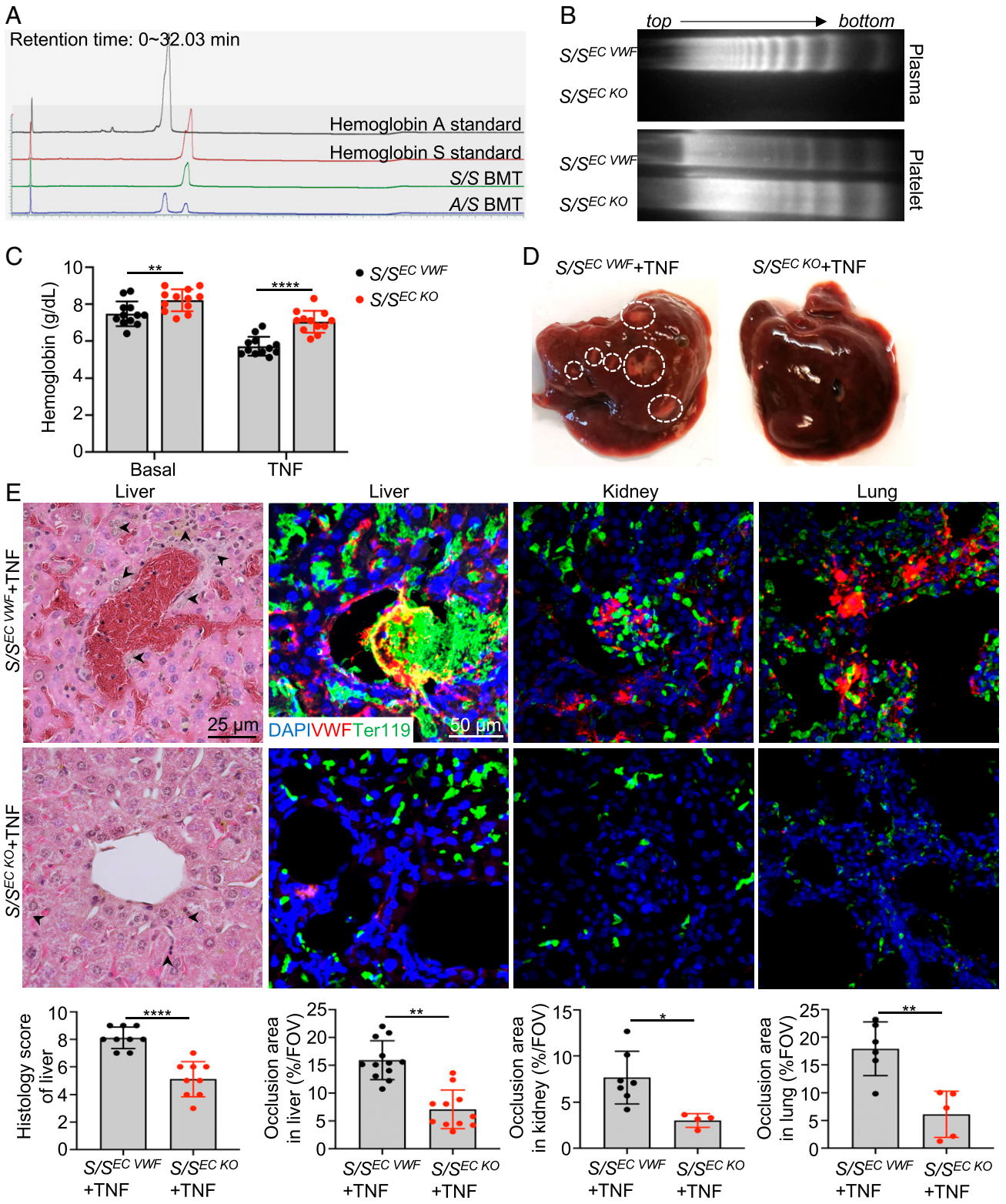


**Fig. 2.** Endothelial VWF deletion improves histopathological phenotypes of VOE. (*A*) Four months after bone marrow transplantation, mouse RBCs were lysed to make hemoglobin solution, and the hemoglobin pattern was analyzed using high-performance liquid chromatography. The mice transplanted with *S/S* bone marrow only expressed sickle hemoglobin. The result is representative of eight independent experiments. (*B*) The multimeric pattern of plasma- and platelet-derived VWF in $S/S^{EC\ VWF}$ and $S/S^{EC\ KO}$ mice showed significant reduction in plasma VWF in $S/S^{EC\ KO}$ mice and successful engraftment of donor bone marrow cells. The result represents four independent experiments. (*C*) Improved hemoglobin levels at basal level and after TNF challenge in $S/S^{EC\ KO}$ mice relative to $S/S^{EC\ VWF}$ mice. Each dot represents one mouse. Data represent mean ± SD. $^{**}P < 0.01$; $^{****}P < 0.0001$, repeated measures 2-way ANOVA. (*D*) Representative gross morphology images of livers collected from $S/S^{EC\ VWF}$ and $S/S^{EC\ KO}$ mice at 3 h after TNF-induced VOE. Dashed circles indicate necrotic areas. The result represents four independent experiments. (*E*) Representative images of H&E-stained liver paraffin sections and immunofluorescence images of cryo-sections of liver, kidney, and lung collected from $S/S^{EC\ VWF}$ and $S/S^{EC\ KO}$ mice at 3 h after TNF-induced VOE. Arrowheads indicate inflammatory infiltrates in H&E staining images. Scale bar, 25 μm. $n = 4$ mice per genotype. Cryo-section slides were stained with primary antibodies to VWF and RBCs (Ter119). DAPI, cell nuclear staining. There was massive sickle RBC sequestration in the liver, kidney, and lung of $S/S^{EC\ VWF}$ mice. Scale bar, 50 μm. $n = 4$ mice per genotype. Corresponding histologic scores and quantification of the percentage of vaso-occlusion area per field of view (FOV) using ImageJ are shown at the bottom. Data represent mean ± SD. $^{*}P < 0.05$; $^{**}P < 0.01$; $^{****}P < 0.0001$, two-tailed, unpaired Student's *t* test.

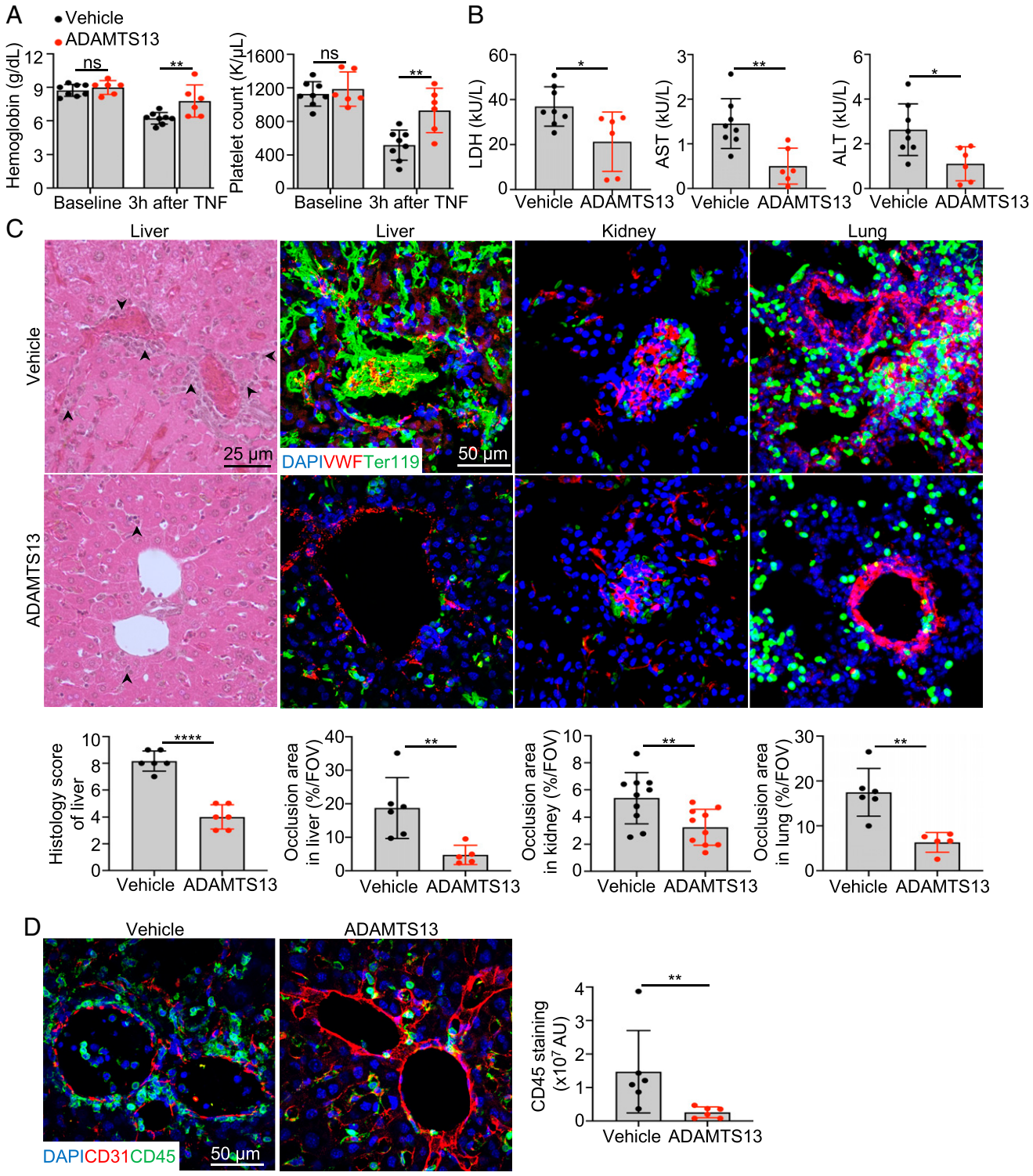


**Fig. 3.** ADAMTS13 injection after VOE reduces pathological changes associated with TNF-induced VOE in SCD mice. (*A*) Comparisons of hemoglobin levels and platelet counts at baseline and 3 h after TNF-induced (500 ng/mouse, intraperitoneally) VOE in vehicle- or ADAMTS13-treated (intravenously, 15 min after VOE induction) *S/S* mice. Data represent mean ± SD. $^{**}P < 0.01$; ns, nonsignificant, repeated measures 2-way ANOVA. (*B*) Plasma levels of tissue damage markers (LDH, AST, and ALT) in vehicle- or ADAMTS13-treated *S/S* mice at 3 h after TNF-induced VOE. Each dot represents one mouse. Data represent mean ± SD. $^{*}P < 0.05$; $^{**}P < 0.01$, two-tailed, unpaired Student's *t* test. (*C*) Representative images of H&E-stained liver paraffin sections and representative immunofluorescence images of cryo-sections of liver, kidney, and lung collected from vehicle- or ADAMTS13-treated *S/S* mice at 3 h after TNF-induced VOE. Representative H&E-stained liver images show reduced vaso-occlusion and inflammatory infiltrates (indicated by arrowheads) in ADAMTS13-treated *S/S* mice compared to vehicle-treated *S/S* mice at 3 h after TNF-induced VOE. Scale bar, 25 μm. Cryo-sections were stained with primary antibodies to VWF and RBCs (Ter119). DAPI, cell nuclear staining. There were decreased vaso-occlusions in ADAMTS13-treated *S/S* mice compared to vehicle-treated *S/S* mice. Scale bar, 50 μm. $n = 5$ mice per treatment group. Corresponding histologic scores and quantification of the percentage of vaso-occlusion area per field of view (FOV) using ImageJ are shown at the bottom. Data represent mean ± SD. $^{**}P < 0.01$; $^{****}P < 0.0001$, two-tailed, unpaired Student's *t* test. (*D*) Representative immunofluorescence images of cryo-sections of livers collected from vehicle- or ADAMTS13-treated *S/S* mice 3 h after TNF-induced VOE. Cryo-sections were stained with primary antibodies to CD31 and CD45. DAPI, cell nuclear staining. Quantification of CD45 staining is shown on the right, and there was reduced inflammatory infiltrates in ADAMTS13-treated *S/S* mice compared to vehicle-treated *S/S* mice. AU, arbitrary unit. Scale bar, 50 μm. $n = 5$ mice per treatment group. Data represent mean ± SD. $^{**}P < 0.01$, Mann-Whitney test.

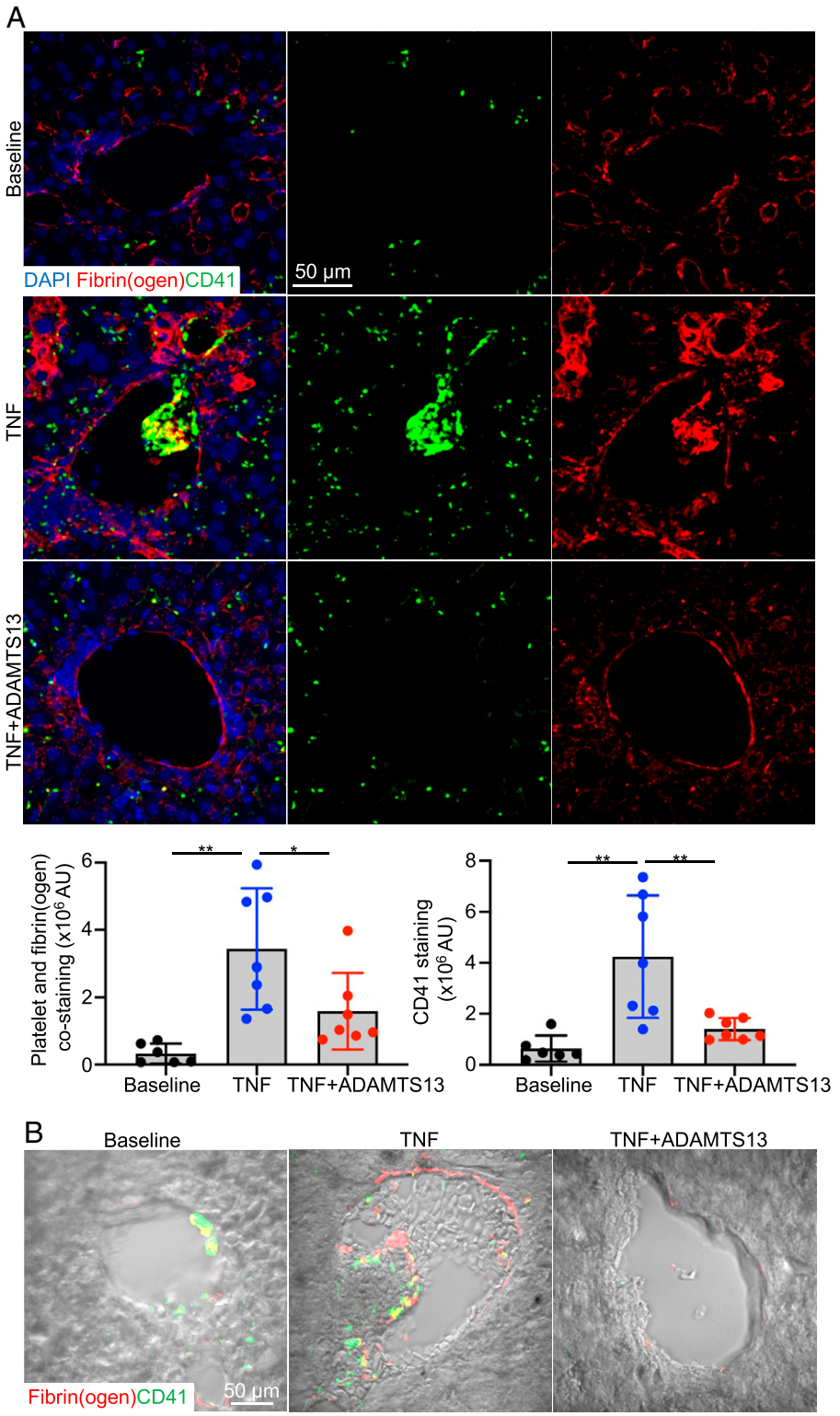


**Fig. 4.** The increased platelet and fibrin deposition in vaso-occlusions of *S/S* mice was reduced by ADAMTS13 treatment. (*A*) Representative immunofluorescence images of livers collected from *S/S* mice at baseline or 3 h after VOE induction (with or without ADAMTS13 treatment). Slides were stained with primary antibodies to platelets (CD41) and fibrin(ogen). DAPI, cell nuclear staining. Bar graphs below represent quantifications of platelet staining and colocalization of platelet and fibrin(ogen). AU, arbitrary unit. Scale bar, 50 μm. $n = 5$ mice per treatment group. Data represent mean ± SD. $^{*}P < 0.05$; $^{**}P < 0.01$, one-way ANOVA. (*B*) Representative DIC images of livers collected from *S/S* mice at baseline or 3 h after VOE induction (with or without ADAMTS13 treatment). Slides were stained with primary antibodies to platelets (CD41) and fibrin(ogen). RBCs were visualized by DIC. Scale bar, 50 μm.

VWF contributes to the pathogenesis of VOE remains unclear. In this study, we found that endothelial VWF is critical for the pathogenesis of VOE in SCD mice. More importantly, the VWF-cleaving protease ADAMTS13 reduces VWF levels, decreases inflammation, ameliorates vaso-occlusion, and alleviates organ damage during VOE in SCD mice Fig. 5. These data indicate the importance of VWF in the pathogenesis of VOE and demonstrate that promoting VWF cleavage by ADAMTS13 may be an efficient therapeutic option for reducing VOE-associated pathological changes.

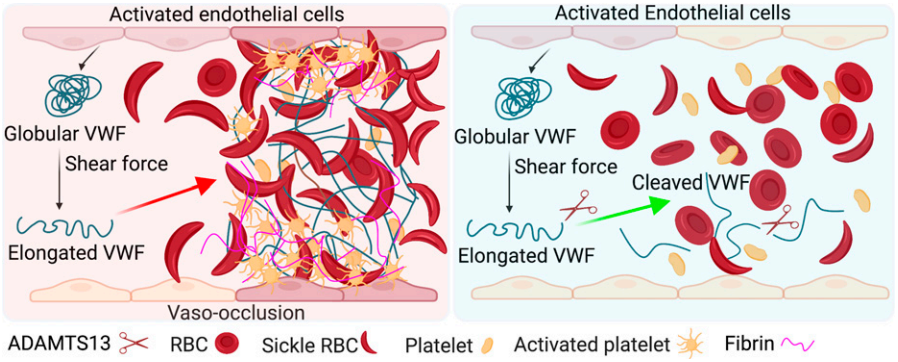


**Fig. 5.** Model depicting role of endothelial VWF in the pathogenesis of VOE (*Left*) and reduction of VOE by ADAMTS13-mediated VWF cleavage (*Right*).

In this study, we used a mouse SCD model ($S/S^{EC\ KO}$) with genetic deletion of VWF specifically in vascular ECs by bone marrow transplantation to demonstrate the biological importance of endothelial VWF in VOE and the ADAMTS13 treatment model to show a potential therapeutic intervention of VOE. On the other hand, although platelet-derived VWF is not essential for normal thrombosis and hemostasis, it is involved in thrombo-inflammatory diseases such as stroke (30). Therefore, ADAMTS13's efficacy may be attributed to its reduction of the activity of VWF derived from both ECs and platelets. In the future, it will be interesting to determine if ADAMTS13 would further reduce VOE in $S/S^{EC\ KO}$ mice, which will help address whether platelet-derived VWF contributes to VOE. It is important to note that $S/S^{EC\ KO}$ mice had reduced expression of endothelial P-selectin (*SI Appendix*, Fig. S11), a component of Weibel–Palade bodies in ECs. P-selectin is known to play a critical role in the pathogenesis of SCD (31). Therefore, other than deficiency of VWF, impaired expression of P-selectin may also contribute to reduced VOE in $S/S^{EC\ KO}$ mice.

In clinical practices, administration of hydroxyurea, L-glutamine, and crizanlizumab can reduce the occurrence of VOE. Unfortunately, a considerable number of individuals with SCD still develop VOE despite these treatments. In addition, treatments such as crizanlizumab do not cause significant improvement in hemolysis (6), which plays an important role in the pathogenesis of VOE (16). Currently, there is no effective treatment for VOE once it occurs (10). A variety of hemolysis products, such as circulating extracellular free hemoglobin and heme, can result in increased inflammation and oxidative stress, thus augmenting VOE (32). We have demonstrated that either deficiency of endothelial VWF or promotion of VWF cleavage by ADAMTS13 reduces hemolysis, improves anemia, and decreases vaso-occlusion in VOE, confirming the role of VWF in VOE-associated pathological changes. Free hemoglobin has been shown to reduce ADAMTS13-mediated cleavage of VWF, which may result in a potential "acquired ADAMTS13 deficiency" state in individuals with SCD (33). In the *S/S* mice treated with ADAMTS13, hemolysis and free hemoglobin levels were reduced compared to vehicle-treated mice. Therefore, supplementing *S/S* mice with exogenous ADAMTS13 can overcome the relative deficiency of endogenous ADAMTS13 and promote VWF cleavage, which may reduce hemolysis and decrease free hemoglobin level, thus breaking the vicious cycle.

Our study demonstrates the therapeutic intervention of VOE using ADAMTS13. During the revisions of this manuscript, a newly published report showed that recombinant ADAMTS13 diminished sickle cell–related organ damage in mice (34). However, in this study, ADAMTS13 was given to mice before hypoxia/reoxygenation-induced VOE, which is a prophylactic rather than therapeutic treatment of VOE. Additionally, a phase 1 clinical trial (NCT03997760) is ongoing to evaluate the safety and pharmacokinetics/pharmacodynamics of recombinant ADAMTS13 in individuals with SCD. Thus, our study provides timely and critical preclinical data demonstrating the potential therapeutic value of ADAMTS13 in the management of VOE for individuals with SCD.

In summary, our study demonstrates the important contribution of endothelial VWF to VOE pathogenesis. ADAMTS13 treatment reduces vaso-occlusion, decreases inflammation, and alleviates organ damage during VOE. Our study shows that promoting VWF cleavage by ADAMTS13 is an effective therapy to reduce VOE-associated pathological changes.

## Materials and Methods

**Mice.** Humanized SCD mice (Townes mice) homozygous for human sickle cell hemoglobin $\beta^S/\beta^S$ (*S/S*) or human WT hemoglobin $\beta^A/\beta^A$ (*A/A*, WT control) (24) were purchased from The Jackson Laboratory. VWF-deficient ($VWF^{-/-}$) mice were a gift from David Ginsburg (University of Michigan Medical School, Ann Arbor, MI) and Long X. Zheng (University of Kansas Medical Center, KS). Mice were housed and maintained at the animal facility (BSL2) of the Oklahoma Medical Research Foundation. All experiments were performed in compliance with protocols approved by the Institutional Animal Care and Use Committee of the Oklahoma Medical Research Foundation.

**Reagents.** ProPac SCX-10 analytical column (4 × 250 mm), 96-well microtiter plate (Immulon 4HBX), 10% Triton X-100, chemiluminescence substrate, and 16% paraformaldehyde (PFA) were purchased from Thermo Fisher Scientific. O-phenylenediamine dihydrochloride substrate and bovine serum albumin were purchased from Sigma-Aldrich. Recombinant mouse TNF and recombinant human ADAMTS13 were purchased from R&D Systems. Enzyme-linked immunosorbent assay (ELISA) kits for IL-1β and IL-12, Alexa Fluor 647 rat monoclonal antibody (mAb) to mouse CD31 (clone MEC13.3), and PE rat mAb to mouse Ter119 (clone TER-119) were purchased from BioLegend. Catalyst chemistry slides for LDH, AST, and ALT were purchased from IDEXX. Seakem Gold agarose was purchased from LONZA. Tissue-Tek optimal cutting temperature (OCT) compound was purchased from Sakura Finetek. Neutral buffered formalin (NBF; 10%) solution was purchased from Azer Scientific. Rat mAb to mouse CD41 (clone MWReg30) and rat mAb to mouse Ter119 (clone TER-119) were purchased from eBioscience. Rabbit polyclonal antibody (pAb) to VWF and rabbit pAb to fibrin(ogen) were purchased from DAKO. Trichrome stain kit, Armenian hamster mAb to mouse CD31 (clone 2H8), and Alexa Fluor 555 donkey pAb to rabbit immunoglobulin (Ig)G (H+L) were purchased from Abcam. Rat mAb to mouse CD45 (clone 30-F11) and rat mAb to mouse P-selectin (clone RB40.34) were purchased from BD Pharmingen. Fluorescein isothiocyanate (FITC) rat mAb to mouse CD41 (clone MWReg30 [RUO]) was purchased from BD Bioscience. Horseradish peroxidase (HRP)–conjugated goat pAb to rabbit IgG (H+L), Alexa Fluor 647 goat pAb to Armenian hamster IgG (H+L), DyLight 488 goat pAb to rat IgG (L), and HRP-conjugated streptavidin were purchased from Jackson ImmunoResearch Inc.

**Mouse Treatment.** VOE was induced by intraperitoneal injection of 500 ng TNF (R&D Systems) (25). In the hypoxia/reoxygenation model, mice were challenged with hypoxia for 10 h (8% $O_2$) followed by reoxygenation for 2 h. For ADAMTS13 treatment, *S/S* mice were intravenously injected with 3 μg recombinant ADAMTS13 (10 pmol/min/μg or 120 IU/kg) (R&D Systems) or vehicle (saline) alone. Mouse blood and tissue samples were collected at 3 h after VOE induction. For the comparison of mouse survival after ADAMTS13/vehicle treatment, mice were monitored for 2 wk.

**Bone Marrow Transplantation.** WT or *VWF*$^{-/-}$ mice were used as recipients. Recipient mice were lethally irradiated using Rad Source RS-2000 series irradiator. A total of 9 Gy irradiation was administered in two equal exposures separated by 3 h. On the other hand, bone marrow nucleated cells were harvested from *S/S* mice. A total of $1 \times 10^7$ donor bone marrow cells were intravenously injected into recipient mice at 3 h after the last irradiation. The engraftment of donor cells was analyzed using VWF multimer analysis and high-performance liquid chromatography at 4 mo after transplantation. VOE was induced in the transplanted mice 4 mo after transplantation, and the mice were euthanized for tissue harvest and subsequent histopathological analysis.

**Complete Blood Count.** Periphery blood was collected from submandibular vein (cheek pouch) into ethylenediaminetetraacetic acid (EDTA)-coated tubes. Complete blood count was measured using automated cell counter Hemavet HV950 (Drew Scientific).

**Blood Chemistry Analysis.** Periphery blood was collected from submandibular vein (cheek pouch) into EDTA-coated tubes and then centrifuged for 10 min at 1,000 *g* and 4 °C to collect plasma. Blood chemistry was measured using LDH, AST, and ALT slides (IDEXX) on Catalyst One Chemistry Analyzer.

**VWF Quantification.** Mouse plasma was prepared as described above. Plasma VWF antigen level was measured using ELISA (Abcam) according to the manufacturer's instructions. Briefly, coating antibody was diluted using bicarbonate/carbonate coating buffer and immobilized on a 96-well microtiter plate (Immulon 4HBX; Thermo Fisher Scientific) overnight at 4 °C. After the plate was blocked on the second day, standards and samples were added and incubated overnight at 4 °C. On the third day, the plate was washed and incubated with the detection antibody, followed by incubation with HRP-conjugated streptavidin (0.5 μg/mL). Next, *o*-phenylenediamine dihydrochloride (OPD) substrate was added, and the reaction was stopped by sulfuric acid. The absorbance was read at 450 nm using FLUOstar Omega microplate reader.

**VWF Multimer Analysis.** Mouse plasma was prepared as described above. Denatured plasma samples were loaded onto 1.3% SDS Seakem Gold agarose (LONZA) gel for electrophoresis. The gel was immunoblotted with rabbit pAb to VWF (DAKO), followed by incubation with HRP-conjugated goat pAb to rabbit IgG (Jackson ImmunoResearch Inc). VWF multimer distribution was visualized by applying chemiluminescence substrate (Thermo Fisher Scientific). Densitometry was analyzed using ImageJ (1.52 q, NIH, Bethesda, MD).

**Histological Analysis.** Mice were perfused with phosphate-buffered saline followed by 4% PFA. Tissues were harvested, fixed in 10% NBF (Azer Scientific) overnight, embedded in paraffin, and sectioned at 5-μm thickness. H&E staining was performed for the evaluation of tissue morphological changes. Slides were imaged using Nikon Eclipse E600 microscope. Blinded histopathological evaluation was performed for H&E staining images. The histologic score was calculated according to vaso-occlusion (none: 0; mild: 1; moderate: 2; severe: 3), inflammation (none: 0; mild: 1; moderate: 2; severe: 3), and cell death (none: 0; mild: 1; moderate: 2; severe: 3).

*Trichrome staining.* Trichrome staining was performed according to the manufacturer's instructions (Abcam). Briefly, formalin-fixed and paraffin-embedded tissues were sectioned at 5-μm thickness. Slides were deparaffinized and then stained sequentially in preheated Bouin's fluid, working Weigert's iron hematoxylin, Biebrich scarlet/acid fuchsin solution, phosphomolybdic/phosphotungstic acid solution, aniline blue solution, and acetic acid solution, followed by dehydration. Stained slides were imaged using a Nikon Eclipse E600 microscope.

**Immunofluorescence Staining.** Mice tissues were harvested and fixed with 4% PFA overnight. After cryopreservation with 20% sucrose, tissues were embedded in OCT (Tissue-Tek, Sakura Finetek). Blocks were sectioned at 20-μm thickness and stained with primary antibodies against VWF (DAKO), CD41 (eBioscience), Ter119 (eBioscience), CD45 (BD Pharmingen), fibrin(ogen) (DAKO), and CD31 (Abcam). Slides were imaged using Nikon C2 confocal microscope. Differential interference contrast (DIC) images were acquired with a Zeiss LSM 710 2-photon microscope.

**High-Performance Liquid Chromatography.** Mouse RBCs were lysed using deionized water, and the derived hemoglobin solution was analyzed using Ultimate 3000 UHPLC (Thermo Fisher Scientific). Analytes were separated on a ProPac SCX-10 analytical column (4 × 250 mm; Thermo Fisher Scientific) at 30 °C. Samples were analyzed using an injection volume of 10 μL at a flow rate of 1.0 mL/min. Solvent A was 50 mM sodium phosphate with 2 mM potassium cyanide, with pH adjusted to 5.6. Solvent B was 50 mM sodium phosphate, 2 mM potassium cyanide, and 0.5 M sodium chloride, with pH adjusted to 5.6. Gradient elution was programmed as follows: 0 to 100% B in 20 min, hold for 2 min.

**Cytokines.** The plasma levels of IL-1β and IL-12 were measured using ELISA according to the manufacturer's instructions (BioLegend). Briefly, capture antibodies against corresponding cytokines were diluted and coated on a 96-well microtiter plate (Immulon 4HBX; Thermo Fisher Scientific) overnight at 4 °C. After blocking, standards and plasma samples were added to the plate and incubated for 2 h at room temperature. Then, the plate was washed, and diluted detection antibodies were added for a 1-h incubation at room temperature, followed by another 1-h incubation with avidin-HRP at room temperature. After washing, TMB substrate was added, and the reaction was stopped by sulfuric acid. Finally, absorbance was read at 450 nm using FLUOstar Omega microplate reader, and the absorbance at 570 nm was subtracted.

**Spinning Disk Intravital Microscopy.** Spinning-disk confocal intravital microscopy was performed following our previously published method (35). At 105 min after TNF-induced VOE, mice were retro-orbitally injected with fluorescence-labeled antibodies: Alexa Fluor 647 rat mAb to mouse CD31 (BioLegend), PE rat mAb to mouse Ter119 (BioLegend), and FITC rat mAb to mouse CD41 (BD Bioscience). In some mice, 3 μg ADAMTS13 was injected 15 min after VOE induction. Mouse surgery started at 2 h after the VOE induction. Mouse anesthesia was induced by ketamine (120 mg/kg)-xylazine (10 mg/kg) (intraperitoneally)) and maintained by 1.5% isoflurane. Mouse body temperature was maintained at 37 °C by a heating pad placed on a surgical stage and coupled to a thermo-controller. Mouse abdominal skin was shaved, and a 2- to 3-cm-long abdominal midline incision was made. The left liver lobe was pulled onto a glass slide supported by a surgical stage using a wet cotton swab. A cover glass was placed on top of the liver and fixed with tape. The exposed liver was superfused with thermo-controlled (37 °C) Hank's balanced salt solution. Vaso-occlusion of the liver sinusoids was visualized and recorded until 3 h after VOE induction using a Nikon ECLIPS E600-FN upright microscope, equipped with an Olympus 40x/0.8W FL water immersion objective lens coupled to a confocal light path based on a modified Yokogawa CSU-X1 head (Yokogawa Electric Corporation); 488-, 561-, and 642-nm excitation lasers were sequentially controlled and merged into a single optic cable and introduced into the CSU-X head. Fluorescence signals were detected through three emission filters of ET525/50, ET605/52, and ET700/75 controlled by an ASI FW-1000 Filterwheel (Applied Scientific Instrumentation) and captured using a 512 × 512–pixel back-thinned EMCCD camera (C9100-13; Hamamatsu).

**Statistics.** Data were analyzed using GraphPad Prism 9. Unless specified specifically, parametric data were analyzed using two-tailed, unpaired Student's *t* test or ANOVA, as appropriate. Nonparametric data were analyzed using Mann-Whitney test. $P < 0.05$ was considered statistically significant.

**Data, Materials, and Software Availability.** All study data are included in the article and/or supporting information.

**ACKNOWLEDGMENTS.** We thank Drs. Rodger P. McEver for critical comments, David Ginsburg and Long X. Zheng for VWF-deficient mice, and Drs. Zhongxin Yu and Kar-Ming Fung for pathological analysis. The study is supported by grants from the NIH (Grant Nos. HL149860 and AHA18CDA34120009).

Author affiliations: [a]Cardiovascular Biology Research Program, Oklahoma Medical Research Foundation, Oklahoma City, OK 73104; [b]Department of Biochemistry and Molecular Biology, University of Oklahoma Health Sciences Center, Oklahoma City, OK 73104; [c]Hematology-Oncology Section, Department of Pediatrics, University of Oklahoma Health Sciences Center, Oklahoma City, OK 73104; and [d]Hematology-Oncology Section, Department of Medicine, University of Oklahoma Health Sciences Center, Oklahoma City, OK 73104

1. D. C. Rees, T. N. Williams, M. T. Gladwin, Sickle-cell disease. *Lancet* **376**, 2018–2031 (2010).
2. M. R. DeBaun *et al.*, Decreased median survival of adults with sickle cell disease after adjusting for left truncation bias: A pooled analysis. *Blood* **133**, 615–617 (2019).
3. D. Manwani, P. S. Frenette, Vaso-occlusion in sickle cell disease: Pathophysiology and novel targeted therapies. *Blood* **122**, 3892–3898 (2013).
4. L. V. Parise, N. Berliner, Sickle cell disease: Challenges and progress. *Blood* **127**, 789 (2016).
5. D. K. Kaul *et al.*, Monoclonal antibodies to αVβ3 (7E3 and LM609) inhibit sickle red blood cell-endothelium interactions induced by platelet-activating factor. *Blood* **95**, 368–374 (2000).
6. K. I. Ataga *et al.*, Crizanlizumab for the prevention of pain crises in sickle cell disease. *N. Engl. J. Med.* **376**, 429–439 (2017).
7. Y. Niihara *et al.*; Investigators of the Phase 3 Trial of l-Glutamine in Sickle Cell Disease, A phase 3 trial of l-glutamine in sickle cell disease. *N. Engl. J. Med.* **379**, 226–235 (2018).
8. S. Charache *et al.*; Investigators of the Multicenter Study of Hydroxyurea in Sickle Cell Anemia, Effect of hydroxyurea on the frequency of painful crises in sickle cell anemia. *N. Engl. J. Med.* **332**, 1317–1322 (1995).
9. E. Du, M. Diez-Silva, G. J. Kato, M. Dao, S. Suresh, Kinetics of sickle cell biorheology and implications for painful vasoocclusive crisis. *Proc. Natl. Acad. Sci. U.S.A.* **112**, 1422–1427 (2015).
10. S. Chaturvedi, M. R. DeBaun, Evolution of sickle cell disease from a life-threatening disease of children to a chronic disease of adults: The last 40 years. *Am. J. Hematol.* **91**, 5–14 (2016).
11. L. L. Swystun *et al.*, Genetic determinants of VWF clearance and FVIII binding modify FVIII pharmacokinetics in pediatric hemophilia A patients. *Blood* **134**, 880–891 (2019).
12. B. Sadler, P. A. Christopherson, G. Haller, R. R. Montgomery, J. Di Paola, von Willebrand factor antigen levels are associated with burden of rare nonsynonymous variants in the VWF gene. *Blood* **137**, 3277–3283 (2021).
13. A. Yee *et al.*, A von Willebrand factor fragment containing the D′D3 domains is sufficient to stabilize coagulation factor VIII in mice. *Blood* **124**, 445–452 (2014).
14. C. Faes *et al.*, Red blood cells modulate structure and dynamics of venous clot formation in sickle cell disease. *Blood* **133**, 2529–2541 (2019).
15. T. M. Wick *et al.*, Unusually large von Willebrand factor multimers increase adhesion of sickle erythrocytes to human endothelial cells under controlled flow. *J. Clin. Invest.* **80**, 905–910 (1987).
16. J. Chen *et al.*, The rate of hemolysis in sickle cell disease correlates with the quantity of active von Willebrand factor in the plasma. *Blood* **117**, 3680–3683 (2011).
17. V. van der Land *et al.*, Markers of endothelial dysfunction differ between subphenotypes in children with sickle cell disease. *Thromb. Res.* **132**, 712–717 (2013).
18. E. M. Novelli *et al.*, Thrombospondin-1 inhibits ADAMTS13 activity in sickle cell disease. *Haematologica* **98**, e132–e134 (2013).
19. J. W. R. Sins *et al.*, Dynamics of von Willebrand factor reactivity in sickle cell disease during vaso-occlusive crisis and steady state. *J. Thromb. Haemost.* **15**, 1392–1402 (2017).
20. J. D. Belcher *et al.*, Heme triggers TLR4 signaling leading to endothelial cell activation and vaso-occlusion in murine sickle cell disease. *Blood* **123**, 377–390 (2014).
21. M. Furlan, R. Robles, B. Lämmle, Partial purification and characterization of a protease from human plasma cleaving von Willebrand factor to fragments produced by in vivo proteolysis. *Blood* **87**, 4223–4234 (1996).
22. H. M. Tsai, Physiologic cleavage of von Willebrand factor by a plasma protease is dependent on its conformation and requires calcium ion. *Blood* **87**, 4235–4244 (1996).
23. J. E. Sadler, Pathophysiology of thrombotic thrombocytopenic purpura. *Blood* **130**, 1181–1188 (2017).
24. T. M. Ryan, D. J. Ciavatta, T. M. Townes, Knockout-transgenic mouse model of sickle cell disease. *Science* **278**, 873–876 (1997).
25. J. Chang *et al.*, GMI-1070, a novel pan-selectin antagonist, reverses acute vascular occlusions in sickle cell mice. *Blood* **116**, 1779–1786 (2010).
26. S. Kanaji, S. A. Fahs, Q. Shi, S. L. Haberichter, R. R. Montgomery, Contribution of platelet vs. endothelial VWF to platelet adhesion and hemostasis. *J. Thromb. Haemost.* **10**, 1646–1652 (2012).
27. A. Pathare *et al.*, Cytokine profile of sickle cell disease in Oman. *Am. J. Hematol.* **77**, 323–328 (2004).
28. J. Venugopal, J. Wang, J. Mawri, C. Guo, D. Eitzman, Interleukin-1 receptor inhibition reduces stroke size in a murine model of sickle cell disease. *Haematologica* **106**, 2469–2477 (2021).
29. M. O. S. Carvalho *et al.*, Inflammatory mediators in sickle cell anaemia highlight the difference between steady state and crisis in paediatric patients. *Br. J. Haematol.* **182**, 933–936 (2018).
30. S. Verhenne *et al.*, Platelet-derived VWF is not essential for normal thrombosis and hemostasis but fosters ischemic stroke injury in mice. *Blood* **126**, 1715–1722 (2015).
31. N. M. Matsui *et al.*, P-selectin mediates the adhesion of sickle erythrocytes to the endothelium. *Blood* **98**, 1955–1962 (2001).
32. G. J. Kato, M. H. Steinberg, M. T. Gladwin, Intravascular hemolysis and the pathophysiology of sickle cell disease. *J. Clin. Invest.* **127**, 750–760 (2017).
33. Z. Zhou *et al.*, Haemoglobin blocks von Willebrand factor proteolysis by ADAMTS-13: A mechanism associated with sickle cell disease. *Thromb. Haemost.* **101**, 1070–1077 (2009).
34. P. Rossato *et al.*, Evidence of protective effects of recombinant ADAMTS13* in humanized model for sickle cell disease. *Haematologica* 10.3324/haematol.2021.280233. (2022).
35. Y. Li *et al.*, Sialylation on O-glycans protects platelets from clearance by liver Kupffer cells. *Proc. Natl. Acad. Sci. U.S.A.* **114**, 8360–8365 (2017).